Interaction of two walkers: perturbed vertical dynamics as a source of chaos

Loïc Tadrist,[1] Naresh Sampara,[2] Peter Schlagheck,[3] and Tristan Gilet[1]
[1)] *Microfluidics Lab, Department of Mechanical and Aerospace Engineering, University of Liege, Allée de la découverte 9, 4000 Liège, Belgium* [a)]
[2)] *Faculty of Engineering, University of Nottingham, University Park, Nottingham, NG7 2RD. United Kingdom*
[3)] *IPNAS, CESAM research unit, University of Liege, Allee du 6 Août 15, 4000 Liège, Belgium*

(Dated: 17 July 2018)

Walkers are dual objects comprising a bouncing droplet dynamically coupled to an underlying Faraday wave at the surface of a vibrated bath. In this paper, we study the wave-mediated interaction of two walkers launched at one another, both experimentally and theoretically. Different outcomes are observed, in which either the walkers scatter, or they bind to each other in orbits or promenade-like motions. The outcome is highly sensitive to initial conditions, which is a signature of chaos, though the time during which perturbations are amplified is finite. The vertical bouncing dynamics, periodic for a single walker, is also strongly perturbed during the interaction, owing to the superposition of the wave contributions of each droplet. Thanks to a model based on inelastic balls coupled to Faraday waves, we show that this perturbed vertical dynamics is the source of horizontal chaos in such system.

PACS numbers: 05.45.Pq, 45.50.Jf, 45.50.Dd
Keywords: Walkers, hydrodynamic quantum analogs, wave-particle duality, two-body chaotic interaction, scattering, orbits, grazing bifurcation, inelastic ball

A *walker* is a dual macroscopic object that consists of a bouncing droplet coupled to a local Faraday wave on a vibrated bath. If the bath is unconfined, a single walker will move horizontally in straight line at constant speed. Many recent studies revealed that, in the presence of horizontal confinement, the horizontal trajectory of the walker may become chaotic. The corresponding statistical description is sometimes surprisingly close to what quantum mechanics would predict for a single quantum particle in similar confinement conditions. However, since the droplet is millimeter-sized, it is not a quantum particle: it must obey the deterministic laws of Newton, while quantum mechanics is conventionally seen as probabilistic. Could chaos bridge the gap between these two conceptions? Where does this chaos originate? In this work, we show that the presence of a second walker may generate chaos through a deep perturbation of the internal clock of the walkers: their vertical bouncing dynamics (figure 1). Even if the interaction of the walkers is of finite duration, the outcome is incredibly sensitive to initial conditions.

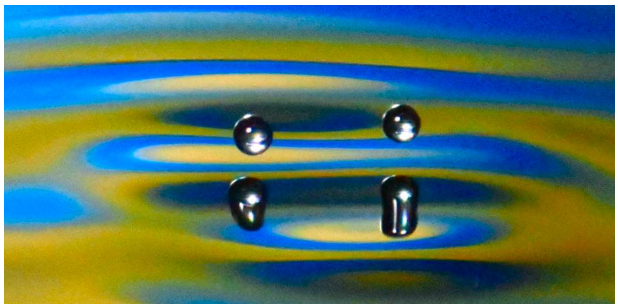

FIG. 1. Walkers are bouncing droplets coupled to Faraday waves on a vibrated liquid bath. Two walkers sufficiently close to each other will interact through the superposition of their waves.

I. INTRODUCTION

In 2005, Y. Couder *et al.*[8] discovered by serendipity that a millimeter-sized droplet can be tightly coupled to waves at the surface of a bath vertically vibrated slightly below the Faraday instability threshold. Thanks to this vibration, the droplet bounces indefinitely without ever coalescing with the bath. Each droplet impact generates some local Faraday waves at the bath surface. Because these waves are still present when the droplet impacts again, some horizontal momentum can be transferred from the waves to the droplet, which starts moving horizontally on the bath[39].

This association of a wave and a particle in the realm of Newton's laws yields behaviors that are reminiscent of quantum particles[5]. In a central force field, a walker experiences orbits with quantized radius and angular momentum[27,28,37]. A similar quantization is seen when the walker moves in a rotating frame[17,23,34]. Interactions of walkers with bath boundaries include non-specular reflexion[41] and tunneling[13,33]. Confinement of the bath

[a)] Electronic mail: loic.tadrist@uliege.be

to a small cavity yields chaotic walker trajectories for which the corresponding statistics is similar to that of a quantum particle in a potential well[19,20,25,42]. The early experiment on Young's slit diffraction of walkers[7] has been recently revisited[1,40] without consensus yet.

Some efforts to rationalize the dynamics of walkers were focused on the hydrodynamic interaction between the droplet and the waves. For a single unconfined walker, the vertical motion of the droplet is locked in a periodic bouncing mode, of period equal to twice the forced vertical vibration of the bath[31,39]. Several generations of hydrodynamic models[14,30,32,39] have been proposed to explain how the waves induce a horizontal motion superimposed to this vertical bouncing. Most of them refer to the *stroboscopic* approximation, which assumes that droplet bouncing remains locked on the bath vibration at all time. Under this assumption, two coupled equations describe the walker's dynamics. First, the horizontal momentum of the droplet responds to the local slope of the wave field. And second, the wave field is enriched by the periodic droplet impacts, often assumed to occur at discrete time and space[17,20]. Since the horizontal displacement of the droplet between successive impacts is much less than the wavelength of emitted Faraday waves, this sum of impacts can be replaced by an integral, which yields a single integro-differential equation for the walker trajectory[6,35]. The motion of a single unconfined walker is then shown to be stable (resp. neutrally stable) to perturbations along (resp. perpendicular to) the direction of motion[35].

Chaotic horizontal trajectories may appear as soon as the walker is confined, either through external forces[23,37] or through bath boundaries[25,42]. The walker is then forced to revisit locations where it previously left standing waves. Eddi *et al.*[14] defined the memory of the wave field as the ratio between the damping time of the waves and the bouncing period. It therefore corresponds to the number of past droplet impacts for which the wave contribution is still significantly present in the current wave field. In other words, this is the number of previous impact positions that are recorded in the wave field. The damping time increases when the Faraday instability threshold is approached from below[26]; it can therefore be tuned by varying the forcing amplitude of the bath. Most of the quantum-like phenomena described above were observed for a memory larger than 20. The mechanisms of transition to chaos for confined walkers were rationalized in Gilet[19], Shirokoff[44], Tambasco *et al.*[45].

The wave-mediated interaction of multiple walkers has received significantly less attention. Protière, Boudaoud, and Couder[39] reported that two identical walkers launched at one another could either scatter or bind to each other. Several bound states were observed, including orbits[36,39] and *promenade* modes where both droplets walk either side by side[2,4] or one behind the other[15]. A difference of mass of the two droplets may yield exotic orbits[38]. At low memory, larger groups of walkers tend to form crystals[16,47], through which phonons can be excited[12].

In this paper, we revisit the wave-mediated interaction of two walkers launched at one another, with the aim of seeing if it can be chaotic and why. Indeed, in this configuration walkers are not confined. So, they are not invited to revisit places where they left waves (with the exception of orbits). Moreover, in the case of scattered trajectories, the interaction time is finite and maybe not sufficient to significantly amplify perturbations of initial conditions. Therefore, the presence of chaos cannot be presumed in this configuration.

Firstly (sections II and III), we describe experiments of walkers launched at one another with various initial conditions, and we characterize the long-timescale horizontal trajectories. We then focus on the short-timescale vertical bouncing dynamics of the droplets during the wave-mediated interaction. Specifically, we aim to check if the *stroboscopic* assumption does still stand though the motion of each walker is not invariant anymore to horizontal translation.

Secondly (sections IV and V), we propose a simple model of this interaction, based on the coupling of the wave field with two inelastic balls. The purpose of this model is to check to which extent potential perturbations of the vertical dynamics could be the origin of some key features observed experimentally. Consequently, the model is designed in order to either let the vertical dynamics free to evolve, or to force this dynamics to comply to the stroboscopic assumption. The model is solved numerically, for different sets of parameters and initial conditions. The model predictions are then compared to experimental observations. In the last section, the origin of chaos in wave-mediated interactions is discussed in the light of the present experiments and model.

The main parameters and variables used through this study are summarized in table I.

II. EXPERIMENTAL SET-UP

The experimental set-up is sketched in figure 2a. A cylindrical reservoir (depth 1.0 cm, inner diameter 28.0 cm) is filled with 6 mm of silicone oil (*Sigma Aldrich*, density 956 kg·m^{-3}, kinematic viscosity $\nu = 20$ cS, surface tension 20.9 kg·s^{-2}). It is tightly screwed on top of an electromagnetic shaker (*V400LT, Data Physics*) that vibrates vertically. The shaker is connected to an amplifier (*DSA5- 2k, Data Physics*) and controlled via a Labview interface through a data acquisition device (*DAQ - National instruments USB 6212*). The elevation of the shaker is $a\cos(2\pi ft)$, where a and f are the amplitude and the frequency of the vibration, respectively. The corresponding maximal acceleration, normalized by gravity g, is $\Gamma = 4\pi^2 f^2 a/g$. The frequency is fixed to $f = 80$ Hz, as in most experiments on walkers[5]. It results in a Faraday wavelength $\lambda_F = 4.75$ mm and a Faraday threshold acceleration of $\Gamma_F = 4.15$. An accelerometer (*PCB, 352C65*) is fixed to the reservoir and connected to the

Parameter	Symbol	Exp.	Model	Units
VARIABLES				
Horizontal position	(x, y) or $\underline{r}$			
Vertical position	z			
Time	t			
EXPERIMENTAL PARAMETERS				
Shaker frequency	f	80	80	Hz
Faraday wavelength	λ_F	4.75	4.75	mm
Shaker amplitude	a	156	192	μm
Shaker acceleration	Γ	4	5.215	
Faraday threshold	Γ_F	4.15	5.30	
Proximity to threshold	$\mathcal{M}$	30	30	
MODEL PARAMETERS				
Impact coefficient	α_1; α_2	-	$[0.1, 1.1]$	μm·s
Velocity coefficient	B	-	$[18,\ 200]$	mm.s^{-1}
INITIAL CONDITIONS				
Impact parameter	b	$[0, 2\lambda_F]$	$[0, 6\lambda_F]$	
Initial walker velocity	V_0	$[5, 12]$	$[1.5, 5]$	mm.s^{-1}
Incident angle	θ_0	$< 5^o$	0^o	
Initial phase difference	$\Delta\phi_0$	$\{0, \pi\}$	0	
OUTPUT VARIABLES				
Wave field elevation	$H(\underline{r}, t)$			
Scattering angle	θ			
Walker position	(x_i, y_i) or $\underline{r}_i$			
Impact time	t_i			
Impact phase	ϕ_i			
Vertical impact speed	v_i			
Next take-off time	t_i^o			

TABLE I. Main parameters and variables. Subscript indices $_1$ and $_2$ refers respectively to walkers 1 and 2. Subscript index $_0$ refers to initial conditions. Subscript index $_i$ refers to the i^{th} impact.

Labview interface. The vibration amplitude is forced to $\Gamma = 4$, which corresponds to $a = 156$ μm, thanks to a feedback loop[43]. The proximity to threshold, defined as $\mathcal{M} = \Gamma_F/(\Gamma_F - \Gamma)$, is then fixed to 30.

The same silicone oil is supplied to home-made piezoelectric dispensers[24,46] that produce droplets of diameter between 700 and 800 μm. The droplets are synchronously released about 1 cm above the oil bath. As soon as they bounce on the bath, they quickly converge to the walking motion (Fig. 2b). The droplet size is hard to measure with sufficient accuracy. However, it strongly influences the walker speed[32], which can be easily determined by image processing with a relative error less than 1%. In constant forcing conditions, Moláček and Bush [32] showed that walker velocity strictly increases with droplet mass. Thus any observed difference in walker speed observed in our experiment can be related to a difference in droplet mass.

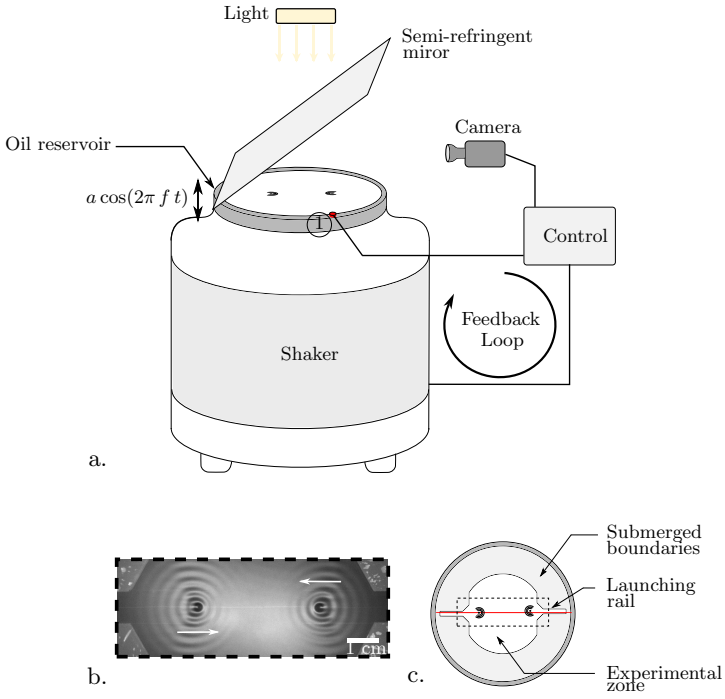

FIG. 2. a. Experimental set-up b. Top view of the experiment as seen by the camera. Both droplets and their surrounding wave field are easily identified. c. Submerged boundaries, designed to launch droplets towards each other.

Boundaries are placed inside the bath in order to confine and guide the walkers (Fig. 2c). They are made of a laser-cut plastic sheet of thickness 4 mm at the bottom of the reservoir. They are thus submerged and consequently they do not radiate any parasitic Faraday wave[3]. The oil layer above these boundaries is sufficiently thin to damp the Faraday waves emitted by the walkers[13]. Two parallel rails of width $2\lambda_F$ are dug into these submerged boundaries in order to launch the droplets towards each other[16]. The rails are either exactly aligned or separated by a distance of about $2\lambda_F$. When the walkers leave the rails, they enter in an experimental zone of diameter 17 cm $\sim 36\lambda_F$ (i.e. much larger than λ_F), where they behave as if they were not confined. They then walk in a straight line until they start interacting with the other walker, i.e. in practice when the walkers are separated by a couple of λ_F.

The oil bath is both lighted and filmed from above thanks to a semi-refringent mirror. Droplet trajectories and associated wave fields are recorded with a camera (*Basler acA2040-180km*) controlled in Labview, at a frequency $f/4$ or $f/2$, with an acquisition phase locked to the shaker vibration. The droplet position at each time is accurately measured in *Matlab 2015b* with a pattern matching technique. About 3000 launches are recorded successively thanks to an automated routine in Labview. The Faraday threshold Γ_F is measured every 5 consecu-

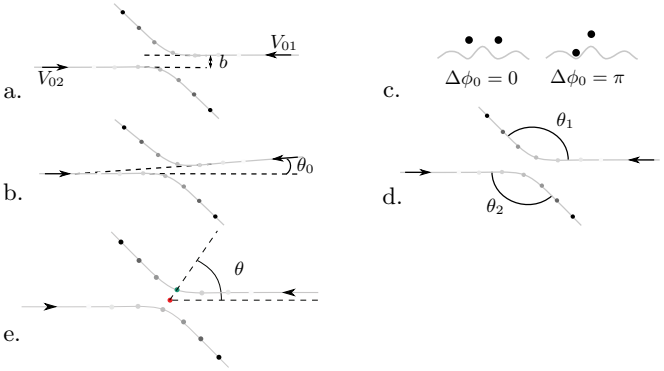

FIG. 3. Parameters that characterize each launch. *a.* Impact parameter b and walker speed (V_{01}, V_{02}). *b.* incidence angle, θ_i. *c.* Initial impact phase shift $\Delta\phi_0$. *d.* Scattering angles θ_1 and θ_2 (in case of a scattering event). *e.* Definition of the limping angle θ. The reference point is the center of mass (•) and the limping position is the green point (•).

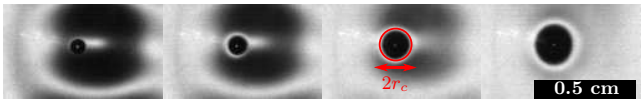

FIG. 4. Top view of the impact of a droplet on the bath and subsequent expansion of the capillary wave. Circles of radius r_c (red) are fitted onto the wave crest (bright circle) and the impact time t_i is defined by linear extrapolation to $r_c = 0$. Time between successive images is 1.22 ms.

tive launches (roughly every 20 minutes) in order to compensate for any slight variations of ambient temperature, and keep $\mathcal{M}$ constant. In practice, an absolute error of $0.002g$ on the forcing acceleration yields a relative error of about 13% on $\mathcal{M}$. Each launch consists of (1) progressively increasing the shaker acceleration to the desired value $\Gamma = (\mathcal{M}-1)\Gamma_F/\mathcal{M}$, (2) generating droplets, (3) record their interaction, and (4) decrease the acceleration down to the point where the droplets coalesce with the bath.

Several input parameters are measured *a posteriori* for each launch (Fig. 3): the initial horizontal speed V_{01} and V_{02} of each walker, the impact parameter b, the incident angle θ_0, and the initial impact phase shift $\Delta\phi_0$ between walkers (0 if rebounds in phase, or π if rebounds in opposition of phase). The impact parameter b is defined as the minimal distance that there would be between both walkers if they were walking at constant speed without mutual interaction. Similarly, the kind of interaction (scattering, orbits and promenades, as defined in figure 5) and the scattering angles (θ_1, θ_2) are measured as output parameters.

There is almost no friction between the droplet and the bath, so the droplet trajectory is very sensitive to parasitic air currents. The experimental zone is here protected from the environment thanks to a cubic box of width 60 cm that surrounds the mirror, the oil reservoir and the droplet dispensers. However, this efficient protection is not infallible. On rare occasions, walker trajectories are seen to deviate from straight lines, even when the walkers are neither close to boundaries nor interacting with each other. The launch is discarded when the unexpected curvature $C > 0.1$ m^{-1}, which corresponds to a lateral deviation of $\Delta x = 0.05\ \lambda_F$ over a walking distance $L = 10\ \lambda_F$. The drag force F_D exerted by air flows on a droplet of mass m must be almost balanced by the inertial force normal to the droplet trajectory, $m\Delta x V_0^2/L^2$. Indeed, the friction between the droplet and the bath is small and walkers are neutrally stable to perturbations in the direction orthogonal to the motion[35]. This drag force, which is then of the order of mCV_0^2, can be compared to the force exerted by the wave field[5], which is estimated as $F_w \sim mgH/\lambda_F$ where H is the characteristic amplitude of the wave field. The ratio $F_D/F_w \sim CV_0^2\lambda_F/(gH)$ is of the order of 5×10^{-4} when a lower bound $H \sim 10$ μm is considered[9]. Consequently, the air drag is of negligible influence to the horizontal walker trajectory when the trajectory curvature of isolated walkers is less than 0.1 m^{-1}.

A zoom on the interaction has been recorded with a high-speed camera (*Phantom MIRO110*) and a macro lens (*Zeiss Milvus 2/100M*) at 8000 fps, i.e. at 200 frames per bouncing period. The impact time t_i and position $\underline{r_i}$ are then inferred from the radial motion of the capillary wave emitted by the droplet impact. The measured radius $r_c(t)$ of the circular wave crest is linearly extrapolated to $r_c(t_i) = 0$ (fig. 4), and its center corresponds to the impact point.

III. EXPERIMENTAL RESULTS

A. Interaction of two walkers

When walkers are sufficiently close to each other, they interact through their waves, since the wave field felt by each is the sum of all the waves previously generated by both. This wave-mediated interaction leads to three main trajectory outputs: two bound states (orbits and promenades) and one free state (scattering). These main outcomes are depicted in Fig. 5. Orbits are usually circular trajectories, where the walkers orbit around their center of mass. The orbital radius is quantified, with successive values approximately separated by half a Faraday wavelength[39], $\lambda_F/2$. Orbits of increasing radius are increasingly less stable[36]. In promenade trajectories, the walkers move together along parallel lines while wobbling in the transverse direction, also approximately separated by a multiple of half a Faraday wavelength[2,4], $\lambda_F/2$. In a scattering event, the interaction time of walkers is finite. Eventually walkers spread apart and stop influencing each other. Their trajectory then becomes a straight line again, whose orientation has been shifted by θ_1 and θ_2 respectively (Fig. 3). Most of the time, scattered an-

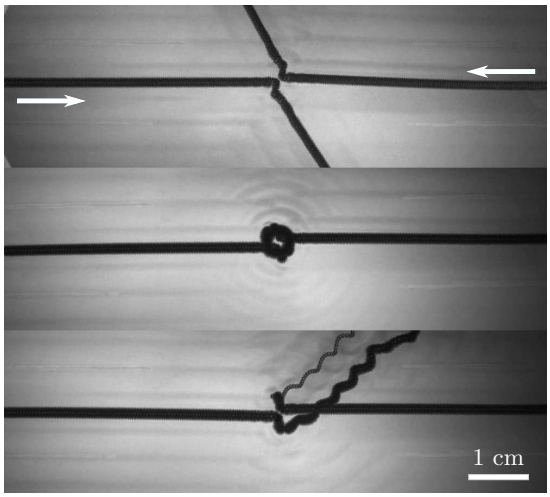

FIG. 5. Time superposition of top views, revealing walker trajectories. Top, middle and bottom lines correspond to scattering, orbit and promenade events.

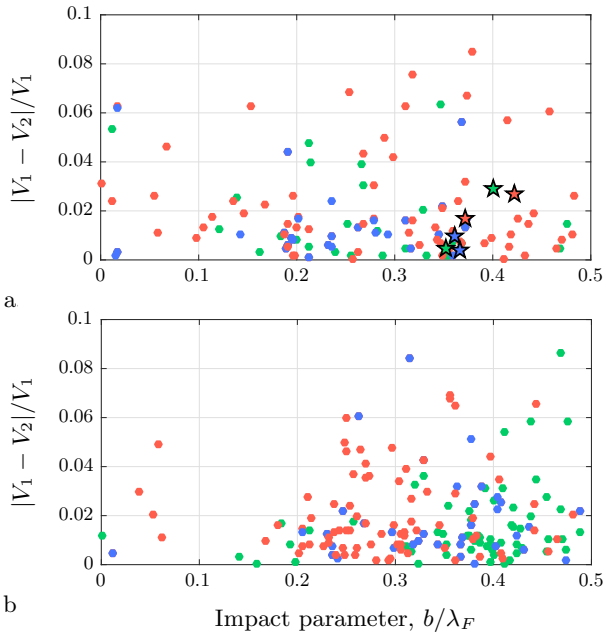

FIG. 6. Experimental outcome of the interaction of two walkers, as a function of the impact parameter b and the relative difference of walking speed $|V_1 - V_2|/V_1$: scattering (•), orbiting (•) and promenade (•). a. Droplets initially bounce with the same impact phase, i.e. $\Delta\phi_0 = 0$. b. Droplets initially bounce with opposite impact phase, i.e. $\Delta\phi_0 = \pi$. The stars correspond to the 6 trajectories represented in figure 7.

gles comply with momentum conservation, which would impose $\theta_1 = \theta_2$ for walkers of identical mass and speed.

Among the 3000 lauches, we could select some for which the memory was $\mathcal{M} = 30$, the mean walker velocity was within $[9, 13]$ mm/s, the incident angle was smaller than 3^o, and the curvature of the approach trajectory was less than 0.1 m^{-1}. The outcome of these launches is represented in figure 6, for both initial phase differences of $\Delta\phi_0 = 0$ and $\Delta\phi_0 = \pi$. Outcomes seem completely mixed on the full range of $b/\lambda_F \in [0, 0.5]$, and no zone therein is dominated by a single outcome. Nevertheless, this mixing might be artificially induced by the pooling of walker trajectories with slightly different mean speed and incident angle.

B. Same initial conditions, different outcomes

We could further select 6 trajectories with extremely similar input parameters: identical impact phase $\Delta\phi_0 = 0$, and small differences in initial velocity ($|V_{01} - V_{02}|/V_{01} < 0.03$), initial velocity (11.2 mm/s $\pm$ 0.5 mm/s), impact parameter ($b = 2\,\mathrm{mm} \pm 0.45$ mm) and incident angle ($\theta_0 = 2^o \pm 0.3^o$). These 6 launches are plotted in Fig. 7b. Remarkably, all three different outcomes are observed in this very narrow range of input parameters. Moreover, several different scattering and promenade angles are produced. The interaction output is here strongly sensitive to initial conditions.

C. Strong perturbations of the vertical dynamics

In order to understand why this deterministic system is so sensitive to initial conditions, we examine the sequence of impact time and position recorded with the high-speed camera, from which the speed V and phase of impact ϕ_i of each walker can be deduced. This phase is measured relative to the shaker motion, with 2π corresponding to one Faraday period $2/f$. A typical interaction is represented in Fig. 8. When walkers are launched towards each other, they first proceed in straight line, at constant speed and impact phase. As they approach each other, they start feeling the other's wave field. Both their velocity and their impact phase fluctuate, and their trajectory deviates from the initial straight line. When the walkers are close to each other, their added contributions to the wave field may result locally in a significantly larger wave amplitude that may be sufficient to destabilize the vertical dynamics of the droplets. Each droplet may then jump lower than expected and already impact the bath after one half of the Faraday period. Both walkers are often destabilized almost at the same time. This event, here called *limping*, corresponds to a strongly premature impact, for which the flight time is decreased by about $1/f$ (figure 9). The appearance of limping can be seen as a grazing bifurcation[10] since it corresponds to the emergence of a new contact event between the droplet and the underlying bath. From there, the vertical bouncing dynamics is completely perturbed, which is seen from the large oscillations in both impact phase and subsequent walker speed. One droplet experiences five major phase changes, while the other experiences two. Ultimately,

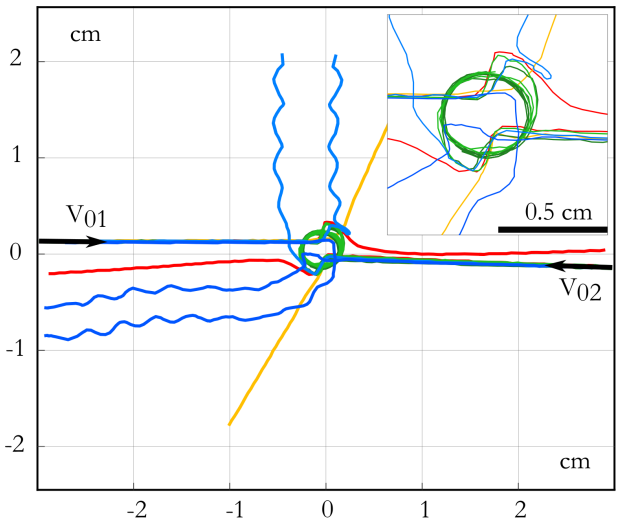

FIG. 7. Superposition of 6 experiments with approximately the same initial conditions, and markedly different outcomes: scattering (red and yellow), orbiting (light and dark green) and promenades (light and dark blue).

the vertical dynamics is stabilized again and both walkers converge to their final fate, which is a promenade in the example of figure 8. However, sometimes one droplet does not converge back to its initial impact phase, but rather to the opposite phase. As far as it could be observed experimentally, the appearance of promenade always involves one droplet ultimately switching to the opposite phase. It can be checked in figure 5, where the thin undulated trace corresponds to one of the outgoing walkers being strobed during flight instead of at impact. Figure 8 reveals how strongly the vertical dynamics is affected during the interaction of two walkers, and it is almost surprising that early stroboscopic models (e.g. in Protière, Boudaoud, and Couder[39]) could qualitatively reproduce some of these outcomes.

Another example of interaction is shown in figure 10. Both particles are launched with speeds $V_{01} = 11.4$ mm/s and $V_{02} = 11.9$ mm/s, with $\Delta\phi_0 = 0$, and with an angle $\theta_0 = 17^o$. Their interaction is complex, and it involves a strong perturbation of the vertical dynamics, especially persistent for one of the walkers. Ultimately, the walkers are scattered away with angles $\theta_1 = 101.8^o$ and $\theta_2 = 38.1^o$, and they both recover their initial speed. The horizontal momentum of the droplets is therefore far from conserved through the interaction.

Limping is not systematically observed for any initial conditions. Nor does it occur at any location. The droplet position during limping events is reported in figure 11. It is defined with the distance $|\underline{r}_1 - \underline{r}_2|$ between both walkers, and the angular position θ. This latter corresponds to the angle between the limping position and the initial position of the droplet, observed from the initial center of mass of both droplets (so $\theta = 0$ when limping is aligned with the initial trajectory), see figure 3e.

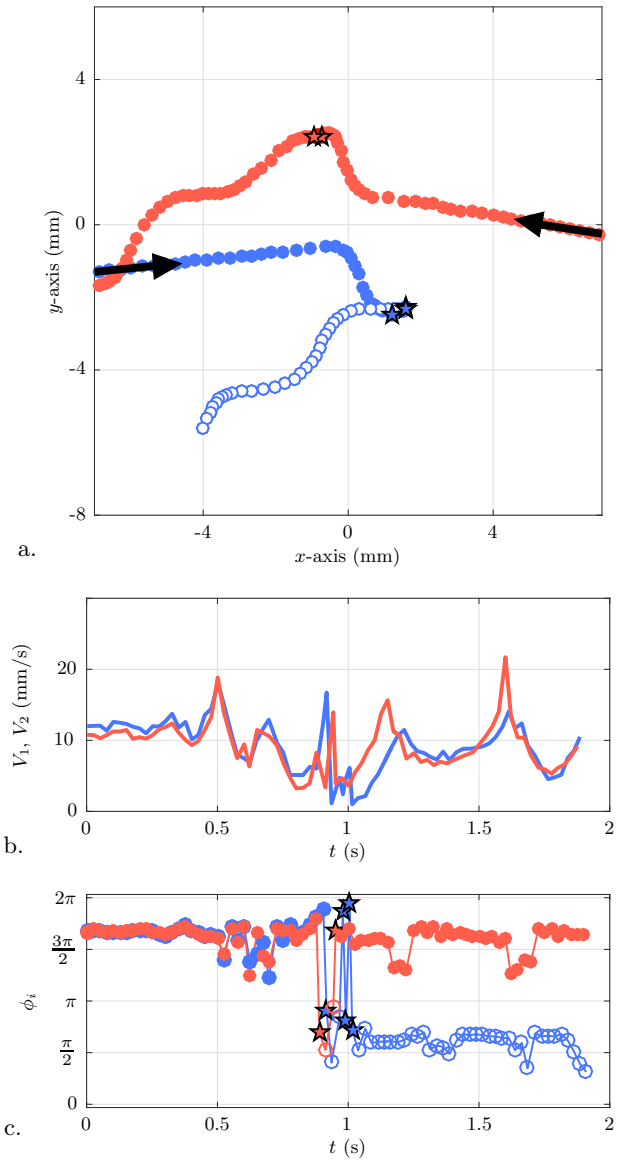

FIG. 8. Example of interaction between two walkers that ends up in a promenade. Data from each droplet are represented in blue and red respectively. a. Horizontal trajectory in the (x, y) plane. Each dot corresponds to one droplet impact. Stars represent limping events, when the impact phase ϕ_i is approximately shifted by π. b. Horizontal instant speed $V_1(t)$ and $V_2(t)$ of each walker. c. Impact phase ϕ_i of each walker.

Three preferential positions of limping can be identified: the angular position $\pi/2$, the distance between walkers $|\underline{r}_1 - \underline{r}_2| \simeq 0.7\lambda_F$, and the angular position π. These preferred limping positions seem relatively independent of the outcome. There might be some constructive interference of the wave contributions of each droplet at these specific locations. A closer look to the wave field, using a schlieren technique for instance, would certainly provide additional clues on the actual conditions necessary to destabilize the walker and induce limping.

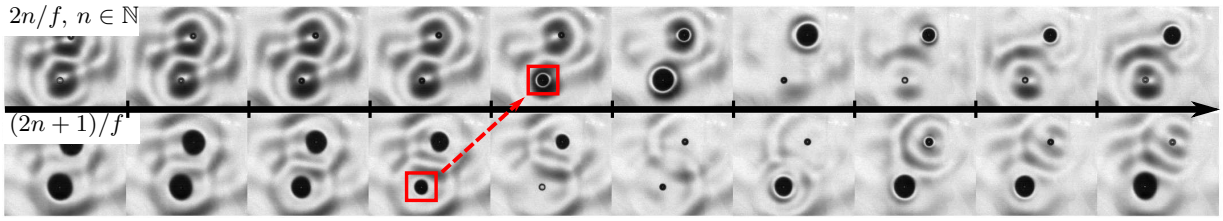

FIG. 9. Chrono-photography of a phase change event. The sequence is read from top to bottom, then from left to right. Successive pictures of the same raw are separated by $1/f = 12.5$ ms and successive pictures of the same line are separated by $2/f = 25$ ms. The first limping event is highlighted within the red box. The limping events each correspond to two impacts on the bath separated by less than $3/(2f)$.

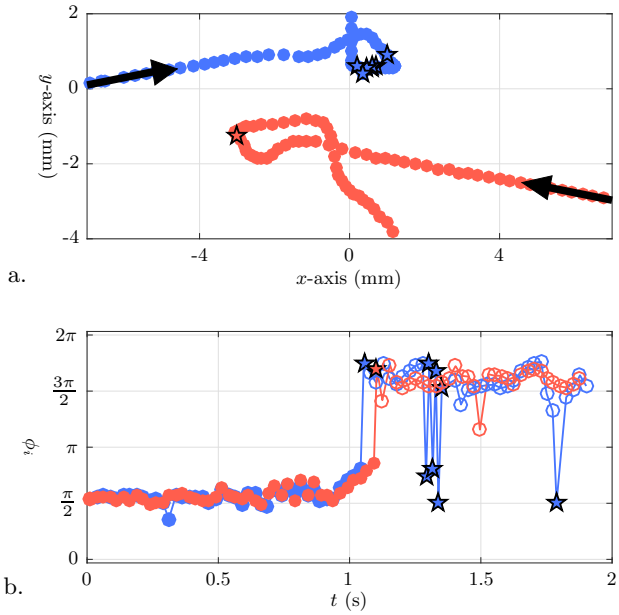

FIG. 10. Complex interaction of two walkers that results in asymmetric scattering. Data from each walker are represented in blue and red respectively. Stars represent limping events, when the impact phase ϕ_i is approximately shifted by π. a. Horizontal trajectory. Each droplet impact corresponds to a colored dot. b. Impact phase ϕ_i of each walker.

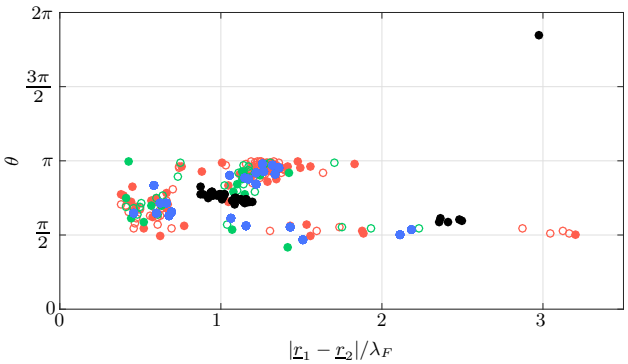

FIG. 11. Horizontal droplet positions at which the first limping event was observed: distance $|\underline{r}_1 - \underline{r}_2|$ between both walkers, vs. angular position θ from the center of mass of the walkers. Colored dots correspond to experimental outcomes: • scattering, • orbits, • promenades. Black dots • correspond to numerical simulations with $\alpha = 11\,10^{-7}$ and $\Delta\alpha = 0.05$. Filled (resp. empty) symbols represent experiments and numerical simulations with $\Delta\phi_0 = 0$ (resp. $\Delta\phi_0 = \pi$).

IV. A SIMPLE MODEL OF WALKERS THAT INCORPORATES THE VERTICAL DYNAMICS

In our experiments, we observed that (i) the interaction of two walkers is strongly sensitive to initial conditions, and that (ii) it often involves strong perturbations of the vertical bouncing dynamics (and so of the impact phase). In order to establish if (ii) is the cause of (i), we will compare the walker trajectories issued from models where the vertical dynamics of each droplet is either forced to a periodic motion, or free to vary in response to the underlying waves.

Most previous models of walkers (e.g. Eddi *et al.*[14], Oza, Rosales, and Bush[35] or Gilet[20]) are strobed, which means that they precisely assume this perfectly periodic vertical motion of the walker, so they do not take into account possible variations of the impact phase. This stroboscopic assumption was possibly convincing for a single walker, but our observations show that it is unrealistic during the interaction of two walkers.

Conversely, the most accurate model of this vertical dynamics, based on a non-linear spring, was developed by Moláček and Bush[31] and implemented together with an appropriate model of Faraday waves in Durey and Milewski[11], Milewski *et al.*[30]. Such complete model involves many additional ingredients in comparison to the strobed models, and it would be difficult to identify which one (if any) is responsible for the strong sensitivity to initial conditions observed with interacting walkers. A simpler bouncing model has been proposed by Galeano-Rios, Milewski, and Vanden-Broeck[18] considering the droplet as a solid sphere bouncing on the bath. However, for all those models, the resulting computation comes at a cost that makes large sets of trajectories out of reach, would they be for some systematic parameter screening or for some statistical analysis.

We here propose to start from a strobed model similar

to that of Eddi *et al.*[14], and then to add the simplest realistic model of vertical dynamics. This latter assumes that each droplet behaves as a completely inelastic ball[22]. Both the inelastic ball and the strobed versions of our model satisfy the same evolution equations for the wave field (section IV A). Only the droplet dynamics is free to vary in the former (section IV B) while it is forced to periodicity in the latter (section IV C). We will then investigate the effect of this vertical droplet dynamics on the sensitivity of walker interactions.

A. Wave field

Each droplet impact on the bath excites some Faraday waves. In a recent paper, we provided an theoretical expression for these waves, based on a careful resolution of Navier-Stokes equations[26]. The wave field corresponding to one droplet impact at position $\underline{r}_i$ is

$$h(r,t) = A\sqrt{\frac{\pi}{Dt}}J_0\left(2\pi\frac{r}{\lambda_F}\right)\exp\left(-\frac{t}{\tau}\right) \exp\left(-\frac{r^2}{4D\,t}\right)\cos\left(\pi f t+\frac{\pi}{4}\right) \qquad (1)$$

where $r = |\underline{r}-\underline{r}_i|$ is the distance to the impact point, J_0 is the Bessel function of the first kind, and other parameters are defined and discussed here below. This wave is modulated in time with a factor $\cos(\pi f t+\pi/4)$ that accounts for oscillations of the surface waves at the Faraday frequency $f/2$.

The forcing frequency $f = 80$ Hz, the Faraday wavelength $\lambda_F = 4.75$ mm and the diffusion coefficient of the spreading wave $D = 5.5\times10^{-4}\,\mathrm{m}^2.\mathrm{s}^{-1}$ were kept identical to the experimental values[26]. In the limit of small viscosity, the characteristic damping time τ of the waves is approximated by[26]

$$\tau \simeq \frac{\mathcal{M}}{\pi\gamma_0 f}\left[1+\frac{\gamma_0^{1/2}}{2}+\frac{\gamma_0}{4}+\mathcal{O}(\gamma_0^{3/2})\right] \qquad (2)$$

with $\gamma_0 \simeq \frac{8\pi\nu}{\lambda_F^2 f}$. Since the proximity to the Faraday threshold is $\mathcal{M} = 30$ in the experiments, we deduce $\tau \simeq 0.574$ s, which corresponds to 23 rebounds in average.

The amplitude A of the wave generated by one droplet impact is modeled as

$$A = \alpha v_i\cos\left(\phi_i+\frac{\pi}{5}\right), \qquad (3)$$

where α is a constant coefficient with dimension $[\mathrm{m}\cdot\mathrm{s}]$, v_i is the impact velocity of the droplet, and $\phi_i = \mathrm{mod}(\pi f t_i, 2\pi)$ the impact phase (with respect to the forced vibration of the shaker) associated to the impact time t_i. The proportionality between amplitude and impact speed results from the conversion of the vertical kinetic energy of the droplet into surface energy[26].

The waves generated by walkers are in the linear regime, where the corresponding amplitude (around 10μm) is much smaller than both the thickness of the boundary layer (300μm) and the Faraday wavelength ($\lambda_F = 4.75$ mm)[26]. Therefore, the total wave field $H(\underline{r},t)$ is simply obtained by summing waves generated at each impact i of droplet j at position $\underline{r}_{ij}$ and impact time t_{ij}:

$$H(\underline{r},t) = \sum_{j\in\{1,2\}}\sum_{i=-\infty}^{n} h(|\underline{r}-\underline{r}_{ij}|, t-t_{ij}). \qquad (4)$$

The waves created at each droplet impact are added to the wave field once the droplet has taken off. In future work, more accurate models of the impact dynamics (*e.g.* Galeano-Rios, Milewski, and Vanden-Broeck[18]) could be implemented to better capture the wave-droplet interaction. These models may suggest alternative hypotheses for the present low-level model of impact dynamics, as for example updating the wave field when the droplet lands instead of when it takes off.

B. Droplet dynamics: the inelastic ball model

In this model we assume that the droplet impact on the bath is perfectly inelastic[22]. At impact, all the kinetic energy (relative to the bath) is lost, and the droplet then sticks to the bath surface. When the absolute acceleration (pointing downwards) becomes smaller than $-g$, the droplet takes off from the bath. It inherits from the instant velocity of the bath at take off. Since air drag is negligible[32], the droplet is then in free fall until the next impact.

Experimentally, the coefficient of restitution of walking droplets is small but not zero[31], so the droplet conserves some of its initial momentum during the impact, i.e. it slightly slides on the bath surface. Moreover, the droplet interacts with the bath for a finite duration, so it inherits from the momentum of the wave averaged over the whole contact duration[32]. We here neglect both of these effects in order to keep our inelastic ball model simple and as close as possible to the strobed model, while being able to qualitatively capture the walker's dynamics.

1. Vertical dynamics

The shaker elevation follows a purely sinusoidal excitation of amplitude a and frequency f. The absolute elevation of the bath surface is then

$$z_\mathrm{b}(\underline{r},t) = a\cos(2\pi\, f\, t) + H(\underline{r},t)\,. \qquad (5)$$

In the regime of large memory, the damping time τ of the wave envelope is much larger than the faraday period $2/f$. Consequently, the time derivatives of $H(\underline{r},t)$ are dominated by the sinusoidal variation of $H(\underline{r},t)$ at frequency $f/2$. Therefore, the local speed and accelera-

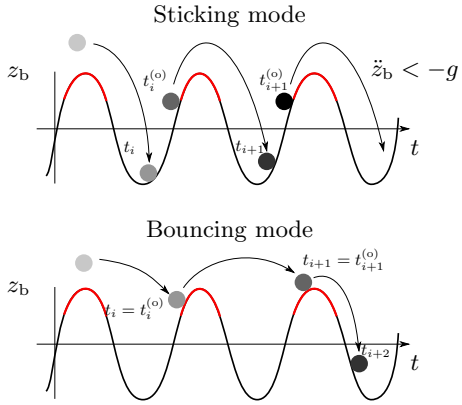

FIG. 12. Vertical dynamics of the perfectly inelastic ball. The curve represents the local elevation of the bath surface. Its red parts correspond to times at which the bath acceleration satisfies $\ddot{z}_b < -g$. Times of impact t_i and take-off $t_i^{(o)}$ of the droplet are indicated. They are distinct in case of sticking, while they are identical in case of bouncing.

tion of the bath surface are:

$$\dot{z}_b(\underline{r},t) \simeq -\pi f \left(2a\sin(2\pi f t) + H(\underline{r},t)\tan\left(\pi f t + \frac{\pi}{4}\right)\right)$$
$$\ddot{z}_b(\underline{r},t) \simeq -\pi^2 f^2 \left(4a\cos(2\pi f t) + H(\underline{r},t)\right) \quad (6)$$

After impact, the droplet will then move along vertically with the bath, while its horizontal position will remain in $\underline{r}_i$. So its vertical position will be $z_d = z_b(\underline{r}_i, t)$.

At time $t_i^{(o)}$ defined by $\ddot{z}_b(\underline{r}_i, t_i^{(o)}) = -g$, the droplet takes off from the bath and inherits its vertical velocity $\dot{z}_b$. Its free fall trajectory then obeys

$$z_d(t) = z_b(\underline{r}_i, t_i^{(o)}) + \dot{z}_b(\underline{r}_i, t_i^{(o)})(t - t_i^{(o)}) - \frac{g}{2}(t - t_i^{(o)})^2 . \quad (7)$$

The droplet impacts the bath again at time t_{i+1} defined as the first time after $t_i^{(o)}$ that satisfies

$$z_d(t_{i+1}) = z_b\left(\underline{r}_i + \dot{\underline{r}}_i(t_{i+1} - t_i^{(o)}), t_{i+1}\right). \quad (8)$$

The impact velocity is then $v_{i+1} = \dot{z}_b(\underline{r}_i, t_{i+1}) - \dot{z}_d(t_{i+1})$. If the acceleration $\ddot{z}_b(\underline{r}_{i+1}, t_{i+1}^{(o)}) > -g$, the droplet sticks again on the bath surface until $t_{i+1}^{(o)} > t_{i+1}$. Otherwise the droplet bounces, i.e. it directly takes off at $t_{i+1}^{(o)} = t_{i+1}$. Both scenarios are illustrated in figure 12. The sticking mode is a fair approximation of the walker's vertical dynamics[31], where the sticking time is a substitute for the experimental contact time.

2. Horizontal dynamics

At each take-off, the droplet inherits its vertical velocity from the velocity of the bath. In the horizontal direction, this speed is assumed to be proportional to the slope of the wave field, at the position of impact $\underline{r}_i$ and at the time of take-off $t_i^{(o)}$, i.e.

$$\dot{\underline{r}}_i = -B\underline{\nabla}H(\underline{r}_i, t_i^{(o)}) \quad (9)$$

A similar assumption is found in most strobed models (e.g.[14,20]). The coefficient B, which dimension is $[\mathrm{m{\cdot}s^{-1}}]$, could possibly depend on the impact velocity v_i. However, we neglect this dependence and consider B constant, for the sake of keeping the model simple and focusing on modifications of the vertical dynamics only.

Equations (1), (4) and (9) contain the core of the horizontal wave-particle coupling. They are present to some extent in almost all existing models of walkers. The two formers capture how each droplet deforms the global wave field, and the latter indicate how each droplet moves in response to the local wave field. The parameter B can therefore be seen as the strength of the coupling between wave and droplet horizontal dynamics.

C. Droplet dynamics: the strobed model

In the strobed model, the vertical dynamics of the droplet is forced to a periodic regime. The impact velocity v_i, the impact phase ϕ_i, the impact time t_i and the take-off time $t_i^{(o)}$ are therefore forced to be constant. For each simulation and set of parameters (α, B), these four constants $(v_i, \phi_i, t_i, t_i^{(o)})$ are chosen identical to the values produced by the inelastic ball model for a single unconfined walker, for which the vertical dynamics converges to a periodic mode. Consequently, as far as isolated walkers are concerned, the inelastic ball and strobed models provide identical predictions. Comparing both models when two walkers interact will therefore shed a focused light on the contribution of the vertical dynamics to the interaction.

D. Parameters and initial conditions

The amplitude of the shaker vibration is fixed to $a = 0.156$ mm in experiments, which determines $\mathcal{M} = 30$ since the Faraday threshold is $\Gamma_F \simeq 4.15$. However, with such amplitude, the inelastic impact model cannot reproduce the walking regime with one impact every two forcing periods. This discrepancy with experiments precisely originates from the perfectly inelastic assumption. The period doubling bifurcation (from one impact every period to one impact every two periods) is generically found in all bouncing ball systems. The forcing amplitude corresponding to this bifurcation increases when the coefficient of restitution decreases[29]. While the bifurcation occurs at $\Gamma \simeq 2.5$ in experiments[32], it only occurs at $\Gamma \simeq 4.5$ in our inelastic model, which corresponds to $a = 0.175$ mm. Fortunately, a can be fixed independently of $\mathcal{M}$ in our model, while both are actually linked

through the Faraday threshold Γ_F in experiments. We have therefore chosen $a = 0.192$ mm (i.e. $\Gamma = 5.125$) for the simulations, which yields a vertical dynamics beyond the period doubling bifurcation, in qualitative agreement with experiments.

Simulations are initialized by *preparing* walkers individually, i.e. as if they were isolated and unconfined on the bath. The inelastic ball model is run for 800 impacts (i.e. more than 30 times the memory) with each walker alone. The walker converges to a constant horizontal speed and a periodic vertical dynamics (from which v_i, ϕ_i, t_i and $t_i^{(o)}$ are determined for the strobed model). The wave field also reaches a steady state, in the framework of the droplet.

These initialized walkers (droplets and associated waves) are then artificially positioned together on the bath, at more than $50\lambda_F$ from each other. They are also reoriented to move towards each other on parallel trajectories ($\theta_0 = 0$) separated by the impact parameter b. They are synchronized in order to initially bounce in phase, i.e. $\Delta\phi_0 = 0$ (fig. 3c). Similar results and conclusions were observed for $\Delta\phi_0 = \pi$, so they are not reported here for the sake of conciseness.

Both models have been extensively tested numerically, mostly for different values of α and B. In previous strobed models (e.g.[20]), the horizontal dynamics of the walker did only depend on the product $A \cdot B$ of the individual wave amplitude A and the horizontal speed coefficient B. So each coefficient could be fixed arbitrarily as long as their product was controlled. In the strobed and inelastic models proposed here, A is not fixed anymore, since it depends on both v_i and ϕ_i. Instead, we focused on keeping the product $\alpha \cdot B = 2\times10^{-8}$ m^2 constant while varying α in the range $[1, 11] \times 10^{-7}$ m·s. The horizontal speed V_0 associated to a single unconfined walker and the wave amplitude $H(r_i^{(o)}, t_i^{(o)})$ right below the walker when it takes off are both reported as functions of α in figure 13. They both increase with α over the considered range, though the increase of H is comparatively much more pronounced than that of V_0.

Both walkers are not necessarily identical. Any difference in mass between the walkers would result in a difference in walking speed ($V_{01} \neq V_{02}$), which can here be captured with a different α for each walker, i.e. $\alpha_1 \neq \alpha_2$. We therefore define an asymmetry coefficient $\Delta\alpha = (\alpha_2 - \alpha_1)/\alpha_1$.

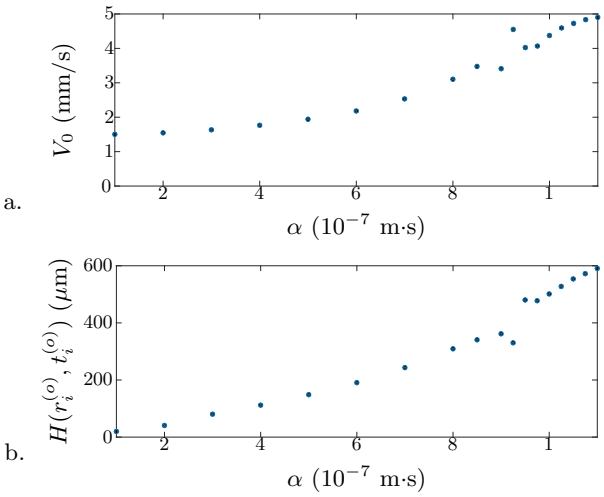

FIG. 13. a. Horizontal velocity of the walker V_0, and b. amplitude of the wave H below the walker at take-off, both as functions of α. The product $\alpha B = 2 \times 10^{-8}$ m^2 is kept constant.

V. MODEL COMPARISON: THE ADDED VALUE OF THE VERTICAL DYNAMICS

A. Trajectories

Typical walker trajectories produced by the inelastic ball model are illustrated in figure 14a. They are qualitatively similar to those observed experimentally. In particular, the computed outputs can be either scattering, orbits or promenades. The four trajectories represented in figure 14a originate from extremely similar initial conditions and input parameters. In one of them, the walkers scatter, but their total momentum, in the sense of individual particles, is not conserved since the output angles θ_1 and θ_2 strongly differ. Similar trajectories were observed experimentally in figure 10. The corresponding impact phase (fig. 14b) always fluctuates during the interaction, which reveals a perturbed vertical dynamics. It then converges to a smaller value for bound states (orbit and promenade) than for free states (scattering), consistently with observations from Oza *et al.*[36] and Arbelaiz, Oza, and Bush[2].

Limping is observed when $\alpha > 10 \times 10^{-7}$ m·s. The position of first limping is represented in figure 11, for the arbitrary choice of parameters $\alpha = 11 \times 10^{-7}$ m·s and $\Delta\alpha = 0.05$. Two preferred zones of limping are identified. The first is at angular position $\theta \simeq \pi/2$, which is very similarly to experiments. The second is when the distance between walkers is around $|\underline{r}_1 - \underline{r}_1| \simeq \lambda_F$, which is larger than the experimental observation $|\underline{r}_1 - \underline{r}_1| \simeq 0.7\lambda_F$.

B. A sensitive outcome

The type of outcome (orbits, promenade, simple and complex scattering) represents a way to assess the sensitivity of the interaction between walkers to initial conditions and parameters. In the maps of figure 15, the outcome is represented as a function of the impact parameter b/λ_F and the relative difference $\Delta\alpha$ between both walkers.

All types of outcome are found in each model configuration. Scattering always dominates at large b. Orbits are present only in certain well-defined intervals of b/λ_F, that correspond to the quantification of orbital radius

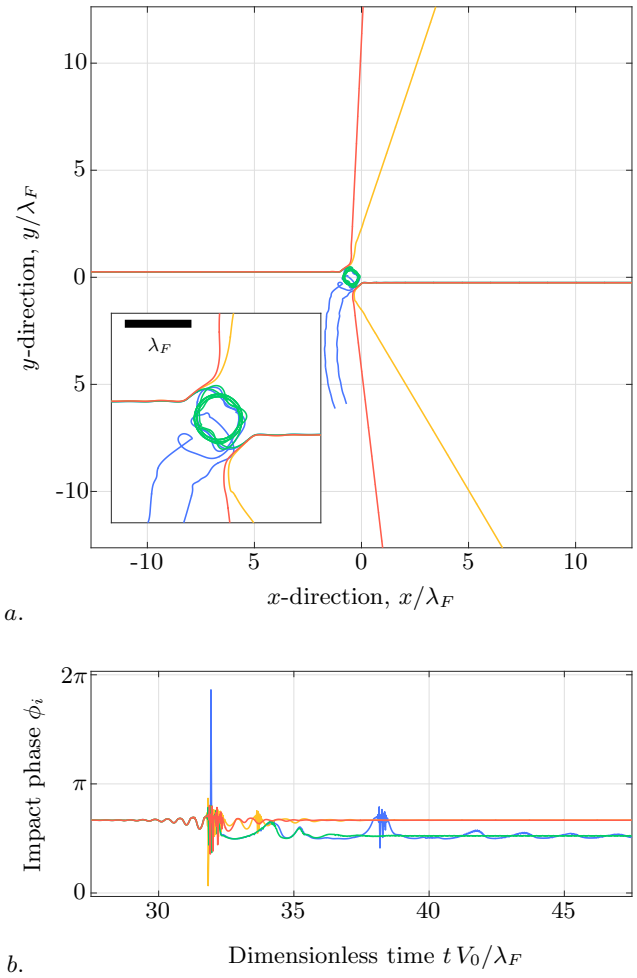

FIG. 14. a. Trajectories computed with the inelastic ball model for $\alpha_1 = 1.1\,10^{-6}$ m·s and slightly different values of $\Delta\alpha$ and b. (red) Scattering for $b/\lambda_F = 2.397\,10^{-3}$ and $\Delta\alpha = 2.717\,10^{-2}$. (green) Orbit for $b/\lambda_F = 2.345\,10^{-3}$ and $\Delta\alpha = 2.717\,10^{-2}$. (blue) Promenade for $b/\lambda_F = 2.345\,10^{-3}$ and $\Delta\alpha = 2.749\,10^{-2}$. (yellow) Complex asymmetric scattering for $b/\lambda_F = 2.397\,10^{-3}$ and $\Delta\alpha = 2.749\,10^{-2}$. b. Evolution of the impact phase ϕ_i for these four trajectories.

already observed in Oza *et al.*[36], Protière, Boudaoud, and Couder[39]. The third interval (around $b/\lambda_F \simeq 3$) is only present for small α, which corroborates the fact that larger orbits tend to be less stable than smaller ones. Promenade modes and complex scattering are only present when $\alpha_1 \neq \alpha_2$, so they only exist when the symmetry between walkers is broken.

The basin of attraction of each outcome is relatively regular for the strobed model, as well as for the inelastic ball model at small α. However, for the inelastic ball model at large α, these basins of attraction appear much less defined. A progressive zoom to the range $b/\lambda_F \in [0.2, 0.5]$ and $\Delta\alpha \in [0.02, 0.03]$ reveals that the basins of attraction are apparently fractal, with a complete interpenetration of orbits and promenades. Moreover, this region of the maps is also frequently subjected to limping events, which again indicates that the vertical dynamics has been strongly perturbed during the interaction.

Figure 16 illustrates how a small region of the (b/λ_F, $\Delta\alpha$) outcome map evolves as α is increased from $3\,10^{-7}$ to $11\,10^{-7}$ m·s. Each map is a 10×10 matrix M_{ij} corresponding to $b_i/\lambda_F \in [0.3, 0.4]$ and $\Delta\alpha_j \in [0.026, 0.029]$. The interlacing of the basins of attraction of orbits and promenades clearly appears for $\alpha > 10^{-6}$ m·s. In order to quantify this heterogeneity of the maps, we define the b-gradient matrix X with elements $X_{ij} = 1$ if $M_{i+1,j} \neq M_{ij}$ and $X_{ij} = 0$ otherwise. Similarly, we define the $\Delta\alpha$-gradient matrix Y with elements $Y_{ij} = 1$ if $M_{i+1,j} \neq M_{ij}$ and $Y_{ij} = 0$ otherwise. We then define the outcome sensitivity as,

$$S_o = \mathrm{Tr}(XX^T) + \mathrm{Tr}(YY^T)\,, \tag{10}$$

and calculate it for each α (Fig. 17b). As already suggested by these maps, this outcome sensitivity S_o significantly increases for $\alpha > 10^{-6}$ m·s (Fig. 17), which is approximately when limping appears.

C. Sensitivity during interaction

Similarly to experiments, the output of the model is strongly sensitive to initial conditions, which is highly reminiscent of chaos. Nevertheless, the amplification time during which perturbations could grow exponentially should be finite here, since output trajectories are stable and non-chaotic on the long term. Therefore, the definition of the Lyapunov exponent must be adapted to consider the divergence of trajectories during some finite amplification time.

This amplification time is not trivially defined. Indeed, it cannot be the interaction time (during which walkers would be closer than a threshold distance), since this latter is infinite for stable orbits and promenades. We here define the amplification time according to the fluctuations of horizontal walker speed $V(t)$ (fig. 18a). These fluctuations are more important when the walkers start interacting and choose between different outcomes. Their amplitude also oscillates with a characteristic frequency of the order of the inverse of the time needed by an isolated walker to travel one Faraday wavelength, i.e. V_0/λ_F. Practically, $\bar{V}(t)$ is computed as the difference of maximal to minimal speed within a time window of width λ_F/V_0 centered on t. The amplification time t_a is defined as the time during which $\bar{V}$ is larger than 50% of its maximal value (fig. 18a). Thanks to this definition, t_a remains finite and focused on the early interaction when a choice of outcome is made, even for stable orbits and promenades where the walker speed may still slightly fluctuate on the long term.

The amplification of perturbations is computed by considering how the trajectories of both walkers $\underline{r}_1(t)$ and $\underline{r}_2(t)$ deviate for two different launches A and B for which

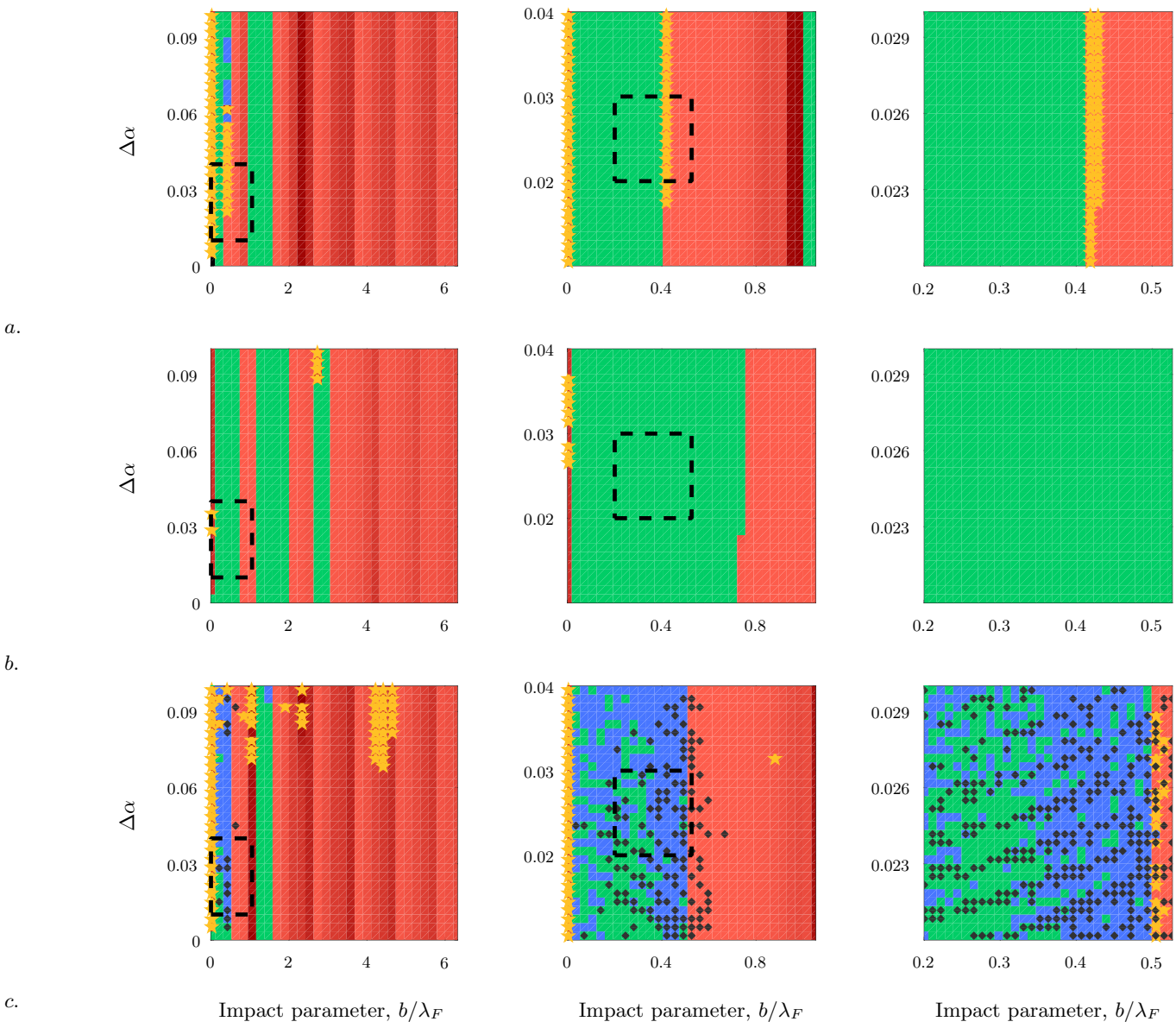

FIG. 15. Interaction outcome (colored) as a function of the impact parameter b/λ_F and the relative difference $\Delta\alpha = (\alpha_2 - \alpha_1)/\alpha_1$ between both walkers. (■) orbits, (■) promenades, (■ to ■) scattering, from small to large scattered angle θ. (★) Complex asymmetric scattering, for which $|\theta_1 - \theta_2| > 10^o$. The occurrence of limping is indicated with an overlying ♦. a. Strobed model, with $\alpha = 11 \times 10^{-7}$m·s. b. Inelastic ball model, with $\alpha = 3 \times 10^{-7}$m·s. c. Inelastic ball model, with $\alpha = 11 \times 10^{-7}$m·s. Second and third columns indicate progressive zooms on a smaller range of b/λ_F and $\Delta\alpha$.

only the impact parameter b differs by $1\,\mu\text{m} = \lambda_F/4750$. The divergence is defined as

$$\delta(t) = \sqrt{|\underline{r}_1^{\text{A}} - \underline{r}_1^{\text{B}}|^2 + |\underline{r}_2^{\text{A}} - \underline{r}_2^{\text{B}}|^2} \tag{11}$$

and its time variation is illustrated in figure 18b. Before both walkers start interacting, δ is almost constant, set to $1\,\mu$m. Within the amplification time window, $\delta(t)$ oscillates, again at a frequency of the order of V_0/λ_F. The envelope of $\delta(t)$ grows almost exponentially with time within this window, which is a signature of local chaos. Finally, outside the amplification time window, the exponential growth of δ stops. For orbits, δ reaches a plateau corresponding to the orbital radius, while for promenade and scattering δ keeps growing, but now linearly with time (because the scattering angles θ_1 and θ_2 slightly differ from A to B). We define the Lyapunov gain as

$$G = \frac{V_0}{\lambda_F} \int_{-\lambda_F/(2V_0)}^{\lambda_F/(2V_0)} \log_{10} \frac{\delta(t_0 + t_a + u)}{\delta(t_0 + u)} \text{d}u \tag{12}$$

where t_0 denotes the beginning of the amplification window (fig. 18b). It corresponds to a total amplification 10^G of perturbations during the interaction time t_a.

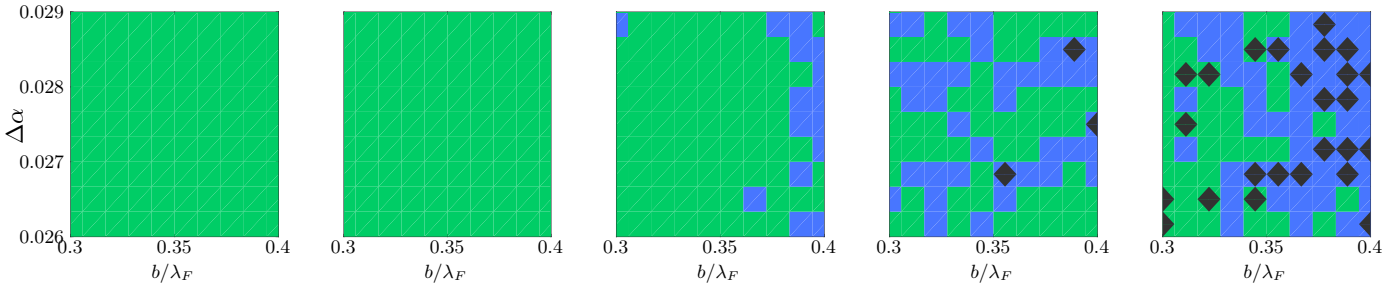

FIG. 16. Evolution of the outcome sensitivity with increasing α. From left to right $\alpha = 3\,10^{-7}$m·s, $\alpha = 8\,10^{-7}$m·s, $\alpha = 10.25\,10^{-7}$m·s, $\alpha = 10.75\,10^{-7}$m·s, $\alpha = 11\,10^{-7}$m·s.

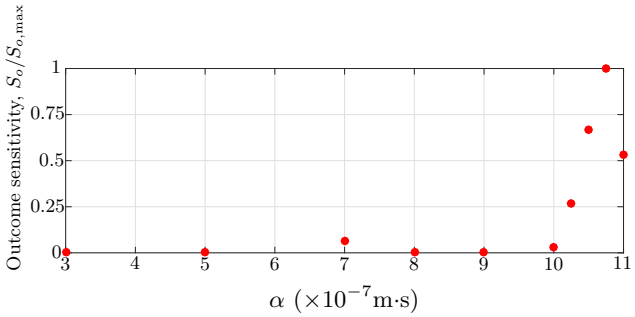

FIG. 17. Variation of the outcome sensitivity S_o, normalized by its maximum value $S_{o,\max} = 5.4\,10^8$, with α.

The variation of G with the impact parameter b is represented in figure 18c, for the inelastic ball model with identical $\alpha = 3.0\,10^{-7}$ s (i.e. waves of amplitude about $80\,\mu$m) for both walkers. This Lyapunov gain is always positive, and it evolves smoothly with b. Peaks of G are nevertheless observed at the transition between outcomes (e.g. here between orbits and scattering). The sensitivity parameter S is defined as the average of G on a homogeneously distributed set of $b/\lambda_F \in [0, 1.05]$:

$$S = \frac{1}{1.05\lambda_F}\int_0^{1.05\lambda_F} G(b)\mathrm{d}b \qquad (13)$$

It expresses the factor by which trajectories separate for a given α, averaged over the impact parameter b. It is aimed to resume the chaotic potential of the interaction in a single number. It is represented as a function of α in figure 18d, for both inelastic ball and strobed models. For the strobed model, S does not vary significantly with α, so the slight divergence of trajectories during the interaction does not really depend on the wave amplitude. By contrast, for the inelastic ball model, S increases with α for $\alpha > 10^{-6}$m·s, meaning that at high wave amplitude, neighbor trajectories strongly diverge during the interaction. For small α, both models yield the same value of S which confirms that, on average, the Lyapunov gain G is insensitive to the vertical dynamics in this range.

Both S_o and S start increasing for $\alpha \gtrsim 10^{-6}$m·s, which is also when limping appears. It corresponds to wave amplitudes larger than about 450 μm, that are sufficient to strongly disturb the vertical dynamics of the perfectly inelastic balls modelled here. However, the vertical dynamics might already be perturbed, to a lesser extent, for $\alpha < 10^{-6}$m·s. In order to analyse this perturbation, we focus on the fluctuations of the impact phase, and we define the standard deviation σ_ϕ,

$$\sigma_\phi = \sqrt{\frac{1}{N-1}\sum_{i=1}^{N}\left(\mathrm{mod}(\phi_i,\pi) - <\phi>\right)^2} \qquad (14)$$

where N is the number of impacts during the amplification window t_a defined previously, and $<\phi> = \sum \mathrm{mod}(\phi_i,\pi)/N$ is the mean value of the impact phase. The modulo π avoids an overweight of permanent phase changes. The impact phase fluctuation σ_ϕ, averaged over all experiments at a given α, is plotted figure 19. It is almost zero for $\alpha < 5\,10^{-7}$m·s, and it increases steadily for larger values of α, without any discontinuity at $\alpha \simeq 10^{-6}$m·s. Therefore, we conclude that the occurrence of limping, as a non-smooth consequence of the perturbation of the vertical dynamics, increases strongly the sensitivity to initial conditions.

VI. DISCUSSION ON THE ORIGIN OF CHAOS

In section III, we observed experimentally that the interaction of two walkers can be chaotic (high sensitivity of the outcome to initial conditions and parameters), and that the associated vertical bouncing dynamics was greatly perturbed during the interaction. This perturbation culminated with the occurrence of limping events, during which a droplet prematurely hits the bath. However, experiments did not reveal if the perturbed vertical dynamics was the cause of this chaos (and thus a necessary condition). Several other phenomena might have participated to the amplification of perturbations. For example, the travelling wave emitted from each impact (on top of the Faraday waves) slightly modifies the wave field, which then appears as a succession of travelling fronts[9]. Those travelling waves might have been sufficiently strong to destabilize the walkers when they were sufficiently close to each other. The air currents, not totally suppressed here, might have also contributed to the apparent stochasticity of the outcome. However this latter cause is unlikely, since it was shown in section II that

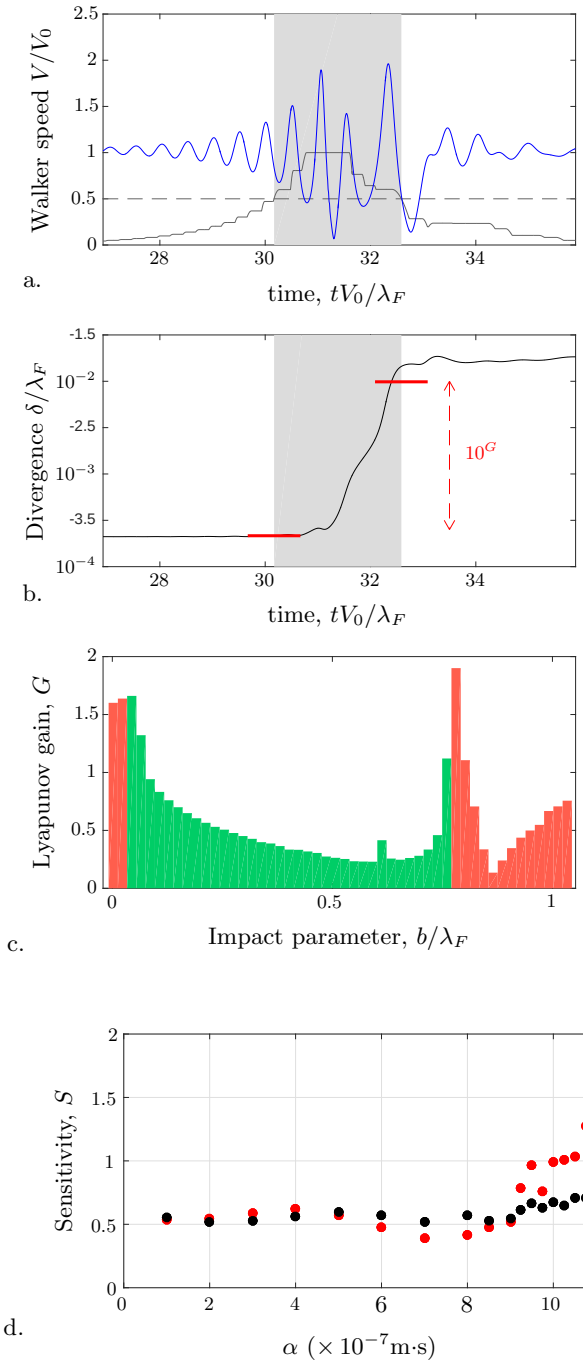

FIG. 18. *a*. Amplification window. (blue line) Normalized horizontal speed V/V_0 of the walker. (black line) Speed fluctuations $\bar{V}/V_0$, low-pass filtered with a cut-off of frequency V_0/λ_F. (grey area) Amplification window of duration t_a, where $\bar{V} > 0.5\max(\bar{V})$. b. Divergence $\delta(t)/\lambda_F$ of two initially similar trajectories. The Lyapunov gain G defined in equation (12) is the vertical red line that indicates the amplification during time t_a. c. Lyapunov gain G as a function of the impact parameter b/λ_F, for $\alpha = 3\,10^{-7}$m·s. The color corresponds to the outcome of the interaction: (red) scattering, or (green) orbits. *d*. Evolution of the sensitivity parameter S as a function of α, for (•) the inelastic ball model, and (•) the strobed model. Dark edged red bullets correspond yo points where limping has been observed.

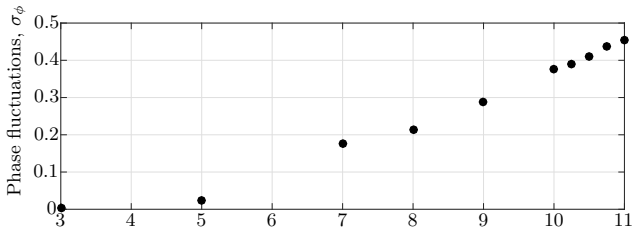

FIG. 19. Fluctuation of the vertical dynamics σ_ϕ as a function of α. Limping is observed when $\alpha \geq 10^{-6}$m·s.

the absence of any significant curvature in the trajectory of isolated walkers was a proof of negligible air drag.

In sections IV and V, we developed a simple model of a wave coupled to a perfectly inelastic particle. We have then shown that this model can reproduce qualitatively the zoology of walker trajectories observed experimentally, and that it exhibits sensitivity to initial conditions only when limping occurs. The latter may therefore be the cause of the former. A similar horizontal chaos induced by strong perturbations of the vertical dynamics was already observed in experiments with walkers forced with multifrequency signals[43]. Limping in itself is a grazing bifurcation, generic to most fly-and-impact systems whose dynamics is piecewise-smooth[10]. It has been observed for partially elastic balls[29], for bouncing droplets on soap films for which the contact time is finite[21], and more importantly in the present experiments on walkers. Limping is therefore not an artefact introduced by the hypotheses of zero contact time and zero coefficient of restitution, and the simplification to a perfectly inelastic ball is not responsible for artificially inducing chaos.

This inelastic assumption strongly decreases the computational time and makes the model simpler to understand. However, it comes at a cost: there is no more quantitative agreement with experiments. In order to reproduce qualitatively similar walking regimes, we needed to increase the forcing acceleration to $\Gamma = 5.125$ (instead of $\Gamma = 4$ in experiments) and to select parameters (α, B) to reach a wave amplitude under the impacting droplet of up to 500 μm (instead of an estimated value between 10 μm and 80 μm in experiments[9,14,26]). With such parameters, the walking velocity (about 5 mm/s) is also twice smaller than in experiments. Nevertheless, the qualitative agreement between the simplified model and experiments is then excellent, in terms of both trajectory outcomes and occurrence of limping. More importantly, it allows to correlate limping to a higher sensitivity to initial conditions. The difference of wave amplitude between our model and experiments may have different sources: (i) the perfectly inelastic hypothesis (which induces an additional dissipation of energy and subsequent stabilization), (ii) the idealisation of a complex interaction of the droplet and the bath during a non-instantaneous impact, (iii) a difference in impact phase, and its consequence on the amplitude of the wave contribution from each impact. Fully understanding this would

require a more in-depth analysis that we think is beyond the scope of this paper. Future work could include the generalization of our study to more realistic models of droplet impact[30] and wave generation[26] for which there would not be an arbitrary choice of parameters (α, B).

VII. CONCLUSION

Walkers are fascinating physical systems in which a particle and a wave are coupled at the macroscopic scale. Although walkers fall within the realm of deterministic Newton's laws, they often exhibit quantum-like behaviors. The apparent stochasticity of walkers is induced by their chaotic dynamics. For confined individual walkers, chaos mostly originates from the memory of the wave field; this latter stores information on the past trajectory of the droplet[19].

In this work, we have observed experimentally that the interaction of two walkers is also highly sensitive to initial parameters. Different outcomes are possible, including scattered trajectories (symmetrical and asymmetric), orbits and promenades. However, the origin of chaos cannot be the same as for confined walkers. Indeed, two interacting walkers do not necessarily explore again regions where they had already left waves. We have seen that horizontal chaos is here concomitant to limping events, which are strong perturbations of the vertical dynamics.

In order to identify the role of the vertical dynamics in generating horizontal chaos, we have proposed a simple model of walkers in which each droplet is resumed to a perfectly inelastic ball. In this model, the vertical dynamics can either be free to obey Newton's laws, or it can be forced into a periodic regime (stroboscopic approximation). We have compared these two vertical dynamics, all other parameters and assumptions being equal. When allowed to, the vertical dynamics was strongly perturbed during the interaction. Limping was observed as soon as the added waves of both walkers were sufficiently high. The model could qualitatively reproduce all the observed outcomes of the interaction. Moreover, the high sensitivity to initial parameters was observed only when limping occurred. Therefore, our work has shown that limping is largely responsible for the chaotic wave-mediated interaction of two walkers.

This second origin of chaotic walker dynamics nicely complements the wave memory mechanism, especially in configurations where walkers do not have the opportunity to revisit places where they had already left standing waves. Among others, the mysterious apparent stochasticity of single walkers passing through slits (diffraction and interference experiments[1,7,40] might find an explanation with some additional chaos from a perturbed vertical dynamics.

ACKNOWLEDGEMENTS

This work was financially supported by the 'Actions de Recherches Concertées (ARC)' of the Wallonia Brussels Federation under contract No. 12-17/02 and by the FNRS grant number CHAR. RECH.-1.B423.18 (Tadrist L.).

[1] Andersen, A., Madsen, J., Reichelt, C., Ahl, S. R., Lautrup, B., Ellegaard, C., Levinsen, M. T., and Bohr, T., "Double-slit experiment with single wave-driven particles and its relation to quantum mechanics," Physical Review E **92**, 013006 (2015).

[2] Arbelaiz, J., Oza, A. U., and Bush, J. W., "Promenading pairs of walking droplets: Dynamics and stability," Physical Review Fluids **3**, 013604 (2018).

[3] Bechhoefer, J., Ego, V., Manneville, S., and Johnson, B., "An experimental study of the onset of parametrically pumped surface waves in viscous fluids," Journal of Fluid Mechanics **288**, 325–350 (1995).

[4] Borghesi, C., Moukhtar, J., Labousse, M., Eddi, A., Fort, E., and Couder, Y., "Interaction of two walkers: Wave-mediated energy and force," Physical Review E **90**, 063017 (2014).

[5] Bush, J. W. M., "Pilot-wave hydrodynamics," Annual Review of Fluid Mechanics **47**, 269–292 (2015).

[6] Bush, J. W. M., Oza, A. U., and Moláček, J., "The wave-induced added mass of walking droplets," Journal of Fluid Mechanics **755**, R7 (2014).

[7] Couder, Y. and Fort, E., "Single-particle diffraction and interference at a macroscopic scale," Physical review letters **97**, 154101 (2006).

[8] Couder, Y., Protiere, S., Fort, E., and Boudaoud, A., "Dynamical phenomena: Walking and orbiting droplets," Nature **437**, 208–208 (2005).

[9] Damiano, A. P., Brun, P.-T., Harris, D. M., Galeano-Rios, C. A., and Bush, J. W., "Surface topography measurements of the bouncing droplet experiment," Experiments in Fluids **57**, 163 (2016).

[10] Di Bernardo, M., Budd, C. J., Champneys, A. R., Kowalczyk, P., Nordmark, A. B., Tost, G. O., and Piiroinen, P. T., "Bifurcations in nonsmooth dynamical systems," SIAM review **50**, 629–701 (2008).

[11] Durey, M. and Milewski, P. A., "Faraday wave–droplet dynamics: discrete-time analysis," Journal of Fluid Mechanics **821**, 296–329 (2017).

[12] Eddi, A., Decelle, A., Fort, E., and Couder, Y., "Archimedean lattices in the bound states of wave interacting particles," EPL (Europhysics Letters) **87**, 56002 (2009).

[13] Eddi, A., Fort, E., Moisy, F., and Couder, Y., "Unpredictable tunneling of a classical wave-particle association," Physical review letters **102**, 240401 (2009).

[14] Eddi, A., Sultan, E., Moukhtar, J., Fort, E., Rossi, M., and Couder, Y., "Information stored in faraday waves: the origin of a path memory," Journal of Fluid Mechanics **674**, 433–463 (2011).

[15] Eddi, A., Terwagne, D., Fort, E., and Couder, Y., "Wave propelled ratchets and drifting rafts," EPL (Europhysics Letters) **82**, 44001 (2008).

[16] Filoux, B., Hubert, M., Schlagheck, P., and Vandewalle, N., "Walking droplets in linear channels," Physical Review Fluids **2**, 013601 (2017).

[17] Fort, E., Eddi, A., Boudaoud, A., Moukhtar, J., and Couder, Y., "Path-memory induced quantization of classical orbits," Proceedings of the National Academy of Sciences **107**, 17515–17520 (2010).

[18] Galeano-Rios, C. A., Milewski, P. A., and Vanden-Broeck, J.-M., "Non-wetting impact of a sphere onto a bath and its application to bouncing droplets," Journal of Fluid Mechanics **826**, 97–127 (2017).

[19] Gilet, T., "Dynamics and statistics of wave-particle interactions in a confined geometry," Physical Review E **90**, 052917 (2014).
[20] Gilet, T., "Quantumlike statistics of deterministic wave-particle interactions in a circular cavity," Physical Review E **93**, 042202 (2016).
[21] Gilet, T. and Bush, J. W., "Chaotic bouncing of a droplet on a soap film," Physical review letters **102**, 014501 (2009).
[22] Gilet, T., Vandewalle, N., and Dorbolo, S., "Completely inelastic ball," Physical Review E **79**, 055201 (2009).
[23] Harris, D. M. and Bush, J. W. M., "Droplets walking in a rotating frame: from quantized orbits to multimodal statistics," Journal of Fluid Mechanics **739**, 444–464 (2014).
[24] Harris, D. M., Liu, T., and Bush, J. W., "A low-cost, precise piezoelectric droplet-on-demand generator," Experiments in Fluids **56**, 83 (2015).
[25] Harris, D. M., Moukhtar, J., Fort, E., Couder, Y., and Bush, J. W., "Wavelike statistics from pilot-wave dynamics in a circular corral," Physical Review E **88**, 011001 (2013).
[26] L. Tadrist, J.-B. Shim, T. G. and Schlagheck, P., "Faraday instability and subthreshold faraday waves: surface waves emitted by walkers," Journal of Fluid Mechanics **848**, 906–945 (2018).
[27] Labousse, M., Oza, A. U., Perrard, S., and Bush, J. W., "Pilot-wave dynamics in a harmonic potential: Quantization and stability of circular orbits," Physical Review E **93**, 033122 (2016).
[28] Labousse, M., Perrard, S., Couder, Y., and Fort, E., "Build-up of macroscopic eigenstates in a memory-based constrained system," New Journal of Physics **16**, 113027 (2014).
[29] Luck, J. and Mehta, A., "Bouncing ball with a finite restitution: chattering, locking, and chaos," Physical Review E **48**, 3988 (1993).
[30] Milewski, P. A., Galeano-Rios, C. A., Nachbin, A., and Bush, J. W. M., "Faraday pilot-wave dynamics: modelling and computation," Journal of Fluid Mechanics **778**, 361–388 (2015).
[31] Moláček, J. and Bush, J. W. M., "Drops bouncing on a vibrating bath," Journal of Fluid Mechanics **727**, 582–611 (2013).
[32] Moláček, J. and Bush, J. W. M., "Drops walking on a vibrating bath: towards a hydrodynamic pilot-wave theory," Journal of Fluid Mechanics **727**, 612–647 (2013).
[33] Nachbin, A., Milewski, P. A., and Bush, J. W. M., "Tunneling with a hydrodynamic pilot-wave model," Phys. Rev. Fluids **2**, 034801 (2017).
[34] Oza, A. U., Harris, D. M., Rosales, R. R., and Bush, J. W., "Pilot-wave dynamics in a rotating frame: on the emergence of orbital quantization," Journal of Fluid Mechanics **744**, 404–429 (2014).
[35] Oza, A. U., Rosales, R. R., and Bush, J. W., "A trajectory equation for walking droplets: hydrodynamic pilot-wave theory," Journal of Fluid Mechanics **737**, 552–570 (2013).
[36] Oza, A. U., Siéfert, E., Harris, D. M., Moláček, J., and Bush, J. W., "Orbiting pairs of walking droplets: Dynamics and stability," Physical Review Fluids **2**, 053601 (2017).
[37] Perrard, S., Labousse, M., Miskin, M., Fort, E., and Couder, Y., "Self-organization into quantized eigenstates of a classical wave-driven particle," Nature communications **5** (2014).
[38] Protiere, S., Bohn, S., and Couder, Y., "Exotic orbits of two interacting wave sources," Physical Review E **78**, 036204 (2008).
[39] Protière, S., Boudaoud, A., and Couder, Y., "Particle–wave association on a fluid interface," Journal of Fluid Mechanics **554**, 85–108 (2006).
[40] Pucci, G., Harris, D. M., Faria, L. M., and Bush, J. W., "Walking droplets interacting with single and double slits," Journal of Fluid Mechanics **835**, 1136–1156 (2018).
[41] Pucci, G., Sáenz, P. J., Faria, L. M., and Bush, J. M. W., "Non-specular reflection of walking droplets," J Fluid Mech **804**, R3 (2016).
[42] Sáenz, P. J., Cristea-Platon, T., and Bush, J. W., "Statistical projection effects in a hydrodynamic pilot-wave system," Nature Physics **14**, 315 (2018).
[43] Sampara, N. and Gilet, T., "Two-frequency forcing of droplet rebounds on a liquid bath," Physical Review E **94**, 053112 (2016).
[44] Shirokoff, D., "Bouncing droplets on a billiard table," Chaos: An Interdisciplinary Journal of Nonlinear Science **23**, 013115 (2013).
[45] Tambasco, L. D., Harris, D. M., Oza, A. U., Rosales, R. R., and Bush, J. W., "The onset of chaos in orbital pilot-wave dynamics," Chaos: An Interdisciplinary Journal of Nonlinear Science **26**, 103107 (2016).
[46] Terwagne, D., Ludewig, F., Vandewalle, N., and Dorbolo, S., "The role of the droplet deformations in the bouncing droplet dynamics," Physics of Fluids **25**, 122101 (2013).
[47] Vandewalle, N., Terwagne, D., Mulleners, K., Gilet, T., and Dorbolo, S., "Dancing droplets onto liquid surfaces," Physics of Fluids **18**, 091106 (2006).